
GRAPH INFOCLUST: LEVERAGING CLUSTER-LEVEL NODE INFORMATION FOR UNSUPERVISED GRAPH REPRESENTATION LEARNING

A PREPRINT

Costas Mavromatis

Department of Computer Science and Engineering
University of Minnesota, USA
mavro016@umn.edu

George Karypis

Department of Computer Science and Engineering
University of Minnesota, USA
karypis@umn.edu

ABSTRACT

Unsupervised (or self-supervised) graph representation learning is essential to facilitate various graph data mining tasks when external supervision is unavailable. The challenge is to encode the information about the graph structure and the attributes associated with the nodes and edges into a low dimensional space. Most existing unsupervised methods promote similar representations across nodes that are topologically close. Recently, it was shown that leveraging additional graph-level information, e.g., information that is shared among all nodes, encourages the representations to be mindful of the global properties of the graph, which greatly improves their quality. However, in most graphs, there is significantly more structure that can be captured, e.g., nodes tend to belong to (multiple) clusters that represent structurally similar nodes. Motivated by this observation, we propose a graph representation learning method called Graph InfoClust (GIC), that seeks to additionally capture cluster-level information content. These clusters are computed by a differentiable K -means method and are jointly optimized by maximizing the mutual information between nodes of the same clusters. This optimization leads the node representations to capture richer information and nodal interactions, which improves their quality. Experiments show that GIC outperforms state-of-art methods in various downstream tasks (node classification, link prediction, and node clustering) with a 0.9% to 6.1% gain over the best competing approach, on average.

1 Introduction

Graph structured data naturally emerge in various real-world applications. Such examples include social networks, citation networks, and biological networks. The challenge, from a data representation perspective, is to encode the high-dimensional, non-Euclidean information about the graph structure and the attributes associated with the nodes and edges into a low dimensional embedding space. The learned embeddings (a.k.a. representations) can then be used for various tasks, e.g., node classification, link prediction, community detection, and data visualization. In this paper, we focus on *unsupervised* representation learning methods that estimate node embeddings without using any labeled data but instead employ various self-supervision approaches. These methods eliminate the need to develop task-specific graph representation models, eliminate the cost of acquiring labeled datasets, and can lead to better representations by using large unlabeled datasets.

Many self-supervision approaches ensure that nodes that are close to each other, both in terms of the graph's topology and in terms of their available features, are also close in the embedding space. This is achieved by employing a contrastive loss between pairs of nearby and pairs of distant nodes; e.g., DeepWalk [1], and GraphSAGE [2]. Another self-supervision approach focuses on reconstructing the existing edges of the graph based on the embedding similarity of the incident nodes; e.g., GAE/VGAE [3]. Because preserving neighbor similarities is desired, many of these methods use graph neural network (GNN) encoders, that insert an additional inductive bias that nodes share similarities with their neighbors.

Motivated by the fact that GNN encoders already preserve similarities between neighboring nodes, Deep Graph Infomax (DGI) [4] adopts a self-supervision approach that maximizes the mutual information (MI) between the representation of each node and the *global* graph representation, which is obtained by averaging the representations of the nodes in

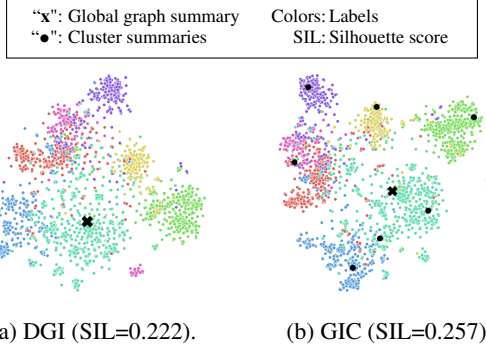


Figure 1: 2D t-SNE projections [7] of the representations learned by DGI and GIC (using 7 clusters) on the CORA citation network [8].

the graph. This encourages the computed node embeddings to be mindful of the global properties of the graph, which improves the representations' quality. DGI has shown to estimate superior node representations [4] and is considered to be among the best unsupervised node representation learning approaches.

By maximizing the mutual information between the representation of a node and that of the global summary, DGI obtains node representations that capture the information content of the entire graph. However, in most graphs, there is significantly more structure that can be captured. For example, nodes tend to belong to (multiple) clusters that represent topologically near-by nodes as well as nodes have similar structural roles but are topologically distant from each other. In such cases, methods that simultaneously maximize the mutual information between the representation of a node and the summary representation of the different clusters that this node belongs to, including that of the entire graph, will allow the node representations to capture the information content of these clusters and thus encode richer structural information.

Motivated by this observation, we developed *Graph InfoClust* (GIC), an unsupervised representation learning method that learns node representations by simultaneously maximizing the mutual information (MI) with respect to the graph-level summary as well as cluster-level summaries. The graph-level summary is obtained by averaging all node representations and the cluster-level summaries by a differentiable K -means clustering [5] of the node representations. The optimization of these summaries is achieved by a noise-contrastive objective, which uses discriminator functions, that discriminate between real and fake samples, as a proxy for estimating and maximizing the MI. The joint computation and optimization of the summaries, promotes both graph-level and cluster-level information and properties to the node representations, which improves their quality. For example, as illustrated in Fig 1, GIC leads to representations that better separate the same-labeled nodes over the representations computed by DGI—the silhouette score (SIL) [6] (see Section 5) of GIC is 0.257 compared to DGI’s 0.222.

We evaluated GIC on seven standard datasets using node classification, link prediction, and clustering as the downstream tasks. Our experiments show that in all but two of the dataset-task combinations, GIC performs better than the best competing approach and its average improvement over DGI is 0.9, 2.6, and 15.5 percentage points for node classification, link prediction, and clustering, respectively. These results demonstrate that by leveraging cluster summaries, GIC is able to improve the quality of the estimated representations.

2 Notation, Definitions, and Problem Statement

We denote vectors by bold lower-case letters and they are assumed to be column vectors (e.g., \mathbf{x}). We also denote matrices by bold upper-case letters (e.g., \mathbf{X}). Symbol $:=$ is used in definition statements. If a matrix \mathbf{X} consists of row vectors $\mathbf{x}_1, \dots, \mathbf{x}_N$, it is denoted as $\mathbf{X} := [\mathbf{x}_1, \dots, \mathbf{x}_N]$.

A graph G that consists of N nodes is defined as $G := \{\mathcal{V}, \mathcal{E}\}$, where $\mathcal{V} := \{n_1, \dots, n_N\}$ is the vertex set and \mathcal{E} is the corresponding edge set. Connectivity is captured by the $N \times N$ adjacency matrix $\mathbf{A} \in \mathbb{R}^{N \times N}$, where $[\mathbf{A}]_{i,j} = 1$ if $(n_i, n_j) \in \mathcal{E}$, and $[\mathbf{A}]_{i,j} = 0$ otherwise. Each node $n_i \in \mathcal{V}$ is also associated with a feature vector $\mathbf{x}_i \in \mathbb{R}^F$. All feature vectors are collected in the feature matrix $\mathbf{X} := [\mathbf{x}_1, \dots, \mathbf{x}_N]$, where $\mathbf{X} \in \mathbb{R}^{N \times F}$.

Let $\mathbf{h}_i \in \mathbb{R}^{F'}$ be an F' -dimensional *node embedding vector* for each $n_i \in \mathcal{V}$. Let $\mathbf{H} := [\mathbf{h}_1, \dots, \mathbf{h}_N]$, such that $\mathbf{H} \in \mathbb{R}^{N \times F'}$ is the *node embedding matrix* of G . The goal of *node representation learning* is to learn \mathbf{H} such that it

preserves both G 's structural information \mathbf{A} and its feature information \mathbf{X} . Once learned, \mathbf{H} can be used as a single input feature matrix for downstream tasks such as node classification, link prediction, and clustering. The problem of node representation learning is equivalent to learning an encoder function, $f : \mathbb{R}^{N \times N} \times \mathbb{R}^{N \times F} \rightarrow \mathbb{R}^{N \times F'}$, that takes the adjacency matrix \mathbf{A} and the feature matrix \mathbf{X} as input and generates node representations \mathbf{H} , namely, $\mathbf{H} = f(\mathbf{A}, \mathbf{X})$.

3 Related work

Non-GNN-based approaches. Early unsupervised approaches relied on matrix factorization techniques, derived by classic dimensionality reduction [9]. They use the adjacency matrix and generate embeddings by factorizing it so that similar nodes have similar embeddings, e.g., Graph factorization [10], GraRep [11], and HOPE [12]. Matrix factorization methods use deterministic measures for node similarity, thus probabilistic models were introduced to offer stochasticity. DeepWalk [1] and node2vec [13] optimize embeddings to encode the statistics of random walks; nodes have similar embeddings if they tend to co-occur on short random walks over the graph. Similar approaches include LINE [14] and HARP [15]. Common limitations of the aforementioned methods is that they are inherently transductive; they need to perform additional optimization rounds to generate embeddings for unseen nodes in the training phase. Generalizing machine learning models (i.e., neural networks) to the graph domain, notably with deep auto-encoders and graph neural networks (GNN), overcame these limitations and made representation learning applicable to large-scale evolving graphs. Deep auto-encoder approaches, such as DNGR [16] and SDNE [17], use multi-layer perceptron encoders to extract node embeddings and multi-layer perceptron decoders to preserve the graph topology.

GNN-based approaches. Graph neural networks (GNN) are machine learning models specifically designed for node embeddings, which operate on local neighborhoods to extract embeddings. GNNs generate node embeddings by *learning* how to repeatedly aggregate neighbors' information. Different GNNs have been developed to promote certain graph properties [18, 19, 20, 2, 21, 22] and primarily differ on how they combine neighbors' information (a survey in [23]). As a result, successful unsupervised methods used GNN encoders to capture topology information. GAE and VGAE [3] use a GNN encoder to generate node embeddings and a simple decoder to reconstruct the adjacency matrix. ARGVA [24] follows a similar schema with VGAE, but learns the data distribution in an adversarial manner [25]. Independently developed, GraphSAGE [26] employs a GNN encoder and a random walk based objective to optimize the node embeddings.

3.1 Deep Graph Infomax

The aforementioned methods share the general idea that nodes that are close in the input data (graph structure or graph structure plus features), should also be as close as possible in the embedding space. Motivated by the fact that GNNs already account for neighborhood information (i.e., are already local-biased), the work of Deep Graph Infomax (DGI) [4] (and inspirational to us) employs an alternative loss function that encourages node embeddings to be mindful of the global structural properties.

The basic idea is to train the GNN-encoder f_{GNN} to maximize the mutual information (MI) [27, 28] between node (fine-grain) representations, i.e., $\mathbf{H} = f_{GNN}(\mathbf{A}, \mathbf{X})$, and a global representation (summary of all representations). This encourages the encoder to prefer the information that is shared across all nodes. If some specific information, e.g., noise, is present in some neighborhoods only, this information would not increase the MI and thus, would not be preferred to be encoded.

Maximizing the precise value of mutual information is intractable, thus, a Jensen-Shannon MI estimator is often used [29, 30], which maximizes MI's lower bound. The Jensen-Shannon-based estimator acts like a standard binary cross-entropy (BCE) loss, whose objective maximizes the expected log-ratio of the samples from the joint distribution (positive examples) and the product of marginal distributions (negative examples). The positive examples are pairings of \mathbf{s} with \mathbf{h}_i of the real input graph $\mathcal{G} := (\mathbf{A}, \mathbf{X})$, but the negatives are pairings of \mathbf{s} with $\tilde{\mathbf{h}}_i$, which are obtained from a fake/corrupted input graph $\tilde{\mathcal{G}} := (\tilde{\mathbf{A}}, \tilde{\mathbf{X}})$ with $\tilde{\mathbf{H}} = f_{GNN}(\tilde{\mathbf{A}}, \tilde{\mathbf{X}})$. Then, a discriminator $\mathcal{D}_1 : \mathbb{R}^{F'} \times \mathbb{R}^{F'} \rightarrow \mathbb{R}$ is used to assign higher scores to the positive examples than the negatives, as in [29, 30].

The Jensen-Shannon-based BCE objective is expressed as

$$\begin{aligned} \mathcal{L}_1 &= \sum_{i=1}^N \mathbb{E}_{(\mathbf{X}, \mathbf{A})} \left[\log \mathcal{D}_1(\mathbf{h}_i, \mathbf{s}) \right] \\ &\quad + \sum_{i=1}^N \mathbb{E}_{(\tilde{\mathbf{X}}, \tilde{\mathbf{A}})} \left[\log (1 - \mathcal{D}_1(\tilde{\mathbf{h}}_i, \mathbf{s})) \right], \end{aligned} \tag{1}$$

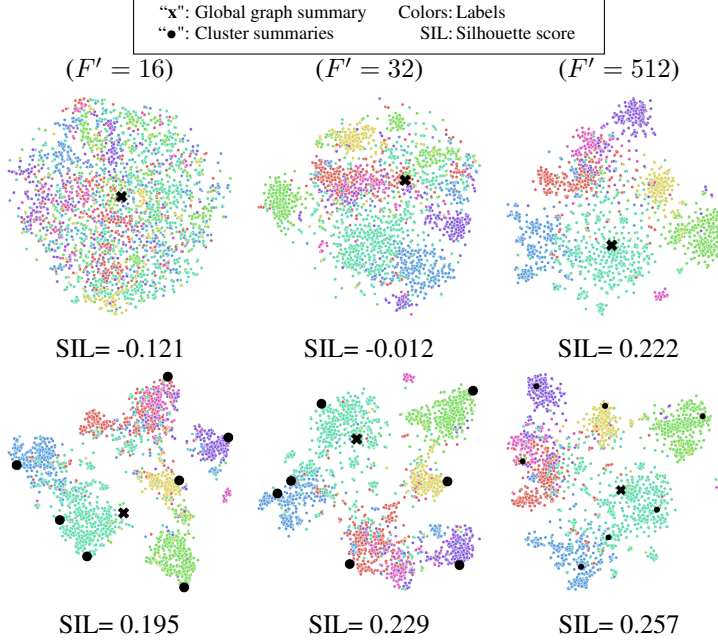


Figure 2: Node representations (after t-SNE 2D projection is applied) and corresponding silhouette scores (SIL) (the higher the better) of leveraging a single graph summary (DGI, top) versus 7 additional cluster summaries (GIC, bottom). GIC is less sensitive to the value of the embedding dimensions F' compared to DGI.

with $\tilde{\mathbf{A}} \in \mathbb{R}^{N \times N}$ and $\tilde{\mathbf{X}} \in \mathbb{R}^{N \times F}$, for simplicity.

This objective is DGI’s main contribution, which leads to superior node representations [4]. As a result, DGI is considered to be among the best unsupervised node representation learning approaches.

4 Graph InfoClust (GIC)

Graph InfoClust relies on a framework similar to DGI’s to optimize the embedding space so that it contains additional cluster-level information content. The novel idea is to learn node representations by maximizing the mutual information between (i) node (fine-grain) representations and the global graph summary, and (ii) node (fine-grain) representations and corresponding cluster (coarse-grain) summaries. This enables the embeddings to be mindful of various structural properties and avoids the pitfall of optimizing the embeddings based on a single vector. We explain this with Figure 2, and show that GIC leads to better representations than DGI, especially when we limit the dimensions F' of the embeddings (its capacity), and thus, the amount of information that can be encoded.

4.1 Overview of GIC

GIC’s overall framework is illustrated in Figure 3. Mutual information is estimated and maximized through discriminator functions that discriminate between positive samples from a real input and negative samples from a fake input $\tilde{\mathcal{G}}$ (Figure 3a), as in [4, 29, 30]. Real node embeddings \mathbf{H} and fake node embeddings $\tilde{\mathbf{H}}$ are obtained by using a graph neural network (GNN) encoder f_{GNN} as $\mathbf{H} = f_{GNN}(\mathbf{A}, \mathbf{X})$ and $\tilde{\mathbf{H}} = f_{GNN}(\tilde{\mathbf{A}}, \tilde{\mathbf{X}})$, respectively (Figure 3b).

The global graph summary $\mathbf{s} \in \mathbb{R}^{1 \times F'}$ is obtained by averaging all nodes’ representations, as in DGI [4]. Cluster summaries $\boldsymbol{\mu}_k$ are obtained by, first, clustering fine-grain representations and, then, computing their summary (average of all nodes within a cluster). Suppose we want to optimize K cluster summaries, so that $\boldsymbol{\mu}_k \in \mathbb{R}^{1 \times F'}$ with $k = 1, \dots, K$ (Figure 3c).

The optimization is achieved by maximizing the mutual information (MI) between nodes within a cluster. In order to estimate and maximize the MI, we compute $\mathbf{z}_i \in \mathbb{R}^{1 \times F'}$ which represents the *corresponding cluster summary* of each node n_i , based on the cluster it belongs to. Then, we can simply maximize the MI between \mathbf{h}_i and \mathbf{z}_i of each node. A discriminator $\mathcal{D}_K : \mathbb{R}^{F'} \times \mathbb{R}^{F'} \rightarrow \mathbb{R}$ is used as a proxy for estimating the MI by assigning higher scores to

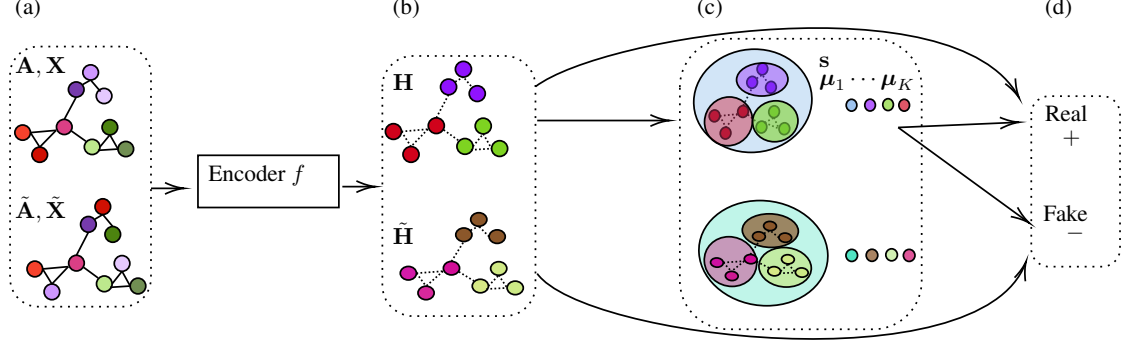


Figure 3: GIC’s framework. (a) A fake input is created based on the real one. (b) Embeddings are computed for both inputs with a GNN-encoder. (c) The graph and cluster summaries are computed. (d) The goal is to discriminate between real and fake samples based on the computed summaries.

positive examples than negatives, as in [4, 29]. We obtain positive examples by pairing \mathbf{h}_i with \mathbf{z}_i from the real graph and negatives by pairing $\tilde{\mathbf{h}}_i$ with \mathbf{z}_i from the fake graph. The proposed objective term is given by

$$\begin{aligned} \mathcal{L}_K = & \sum_{i=1}^N \mathbb{E}_{(\mathbf{X}, \mathbf{A})} \left[\log \mathcal{D}_K(\mathbf{h}_i, \mathbf{z}_i) \right] \\ & + \sum_{i=1}^N \mathbb{E}_{(\tilde{\mathbf{X}}, \tilde{\mathbf{A}})} \left[\log (1 - \mathcal{D}_K(\tilde{\mathbf{h}}_i, \mathbf{z}_i)) \right] \end{aligned} \quad (2)$$

and GIC’s overall objective is given by

$$\mathcal{L} = \alpha \mathcal{L}_1 + (1 - \alpha) \mathcal{L}_K, \quad (3)$$

where $\alpha \in [0, 1]$ controls the relative importance of each component.

4.2 Implementation Details

Fake input. When the input is a single graph, we opt to corrupt the graph by row-shuffling the original features \mathbf{X} as $\tilde{\mathbf{X}} := \text{shuffle}([\mathbf{x}_1, \mathbf{x}_2, \dots, \mathbf{x}_N])$ and $\tilde{\mathbf{A}} := \mathbf{A}$ as proposed by [4] (see Figure 3a). In the case of multiple input graphs, it may be useful to randomly sample a different graph from the training set as negative examples [4].

Cluster and graph summaries. The graph’s summary s in Eq. (1) (and thus in Eq. (3)), is computed as

$$s = \sigma \left(\frac{1}{N} \sum_{i=1}^N \mathbf{h}_i \right), \quad (4)$$

and is essentially the average of all node representations with a nonlinearity $\sigma(\cdot)$; here is the logistic sigmoid, which worked better in our case and in [4].

In Eq. (2), in order to compute \mathbf{z}_i for each node n_i , we apply a weighted average of the summaries of the clusters to which node n_i belongs to, as

$$\mathbf{z}_i = \sigma \left(\sum_{k=1}^K r_{ik} \boldsymbol{\mu}_k \right), \quad (5)$$

where r_{ik} is the degree that node n_i is assigned to cluster k , and is a soft-assignment value (i.e., $\sum_k r_{ik} = 1, \forall i$), and $\sigma(\cdot)$ is the logistic sigmoid nonlinearity.

The cluster summaries $\boldsymbol{\mu}_k$, with $k = 1, \dots, K$, are obtained by a layer that implements a differentiable version of K -means clustering, as in ClusterNet [5]. The ClusterNet layer updates the cluster centers in an end-to-end differentiable manner based on an input objective term, e.g., cluster modularity maximization. Here, we use Eq. (2) to optimize the

clusters, and essentially maximize the intra-cluster mutual information. More precisely, the cluster centroids μ_k are updated by optimizing Eq. (2) via an iterative process by alternately setting

$$\mu_k = \frac{\sum_i r_{ik} \mathbf{h}_i}{\sum_i r_{ik}} \quad k = 1, \dots, K \quad (6)$$

and

$$r_{ik} = \frac{\exp(-\beta \text{sim}(\mathbf{h}_i, \mu_k))}{\sum_k \exp(-\beta \text{sim}(\mathbf{h}_i, \mu_k))} \quad k = 1, \dots, K, \quad (7)$$

where $\text{sim}(\cdot, \cdot)$ denotes a similarity function between two instances and β is an inverse-temperature hyperparameter; $\beta \rightarrow \infty$ gives a binary value for each cluster assignment. All $\mathbf{h}_i, \mathbf{z}_i$, and r_{ik} for each node n_i , and thus μ_k , are jointly optimized and the process is analogous to the typical K -means updates. It was shown that the approximate gradient with respect to the cluster centers can be calculated by unrolling a single (the last one) iteration of the forward-pass updates [5]. This enables the final cluster output to be computed in an end-to-end fashion.

Discriminators. As the discriminator function \mathcal{D}_1 , which is a proxy for estimating the MI between node representations and the graph summary, we use a bilinear scoring function, as proposed in [4], followed by a logistic sigmoid nonlinearity, which convert scores into probabilities, as

$$\mathcal{D}_1(\mathbf{h}_i, \mathbf{s}) = \sigma(\mathbf{h}_i^T \mathbf{W} \mathbf{s}), \quad (8)$$

with \mathbf{W} being a learnable scoring matrix.

Moreover, we use an inner product similarity, followed by a logistic sigmoid nonlinearity $\sigma(\cdot)$, as the discriminator function \mathcal{D}_K for estimating the MI between node representations and their cluster summaries as

$$\mathcal{D}_K(\mathbf{h}_i, \mathbf{z}_i) = \sigma(\mathbf{h}_i^T \mathbf{z}_i). \quad (9)$$

Here, we replace the bilinear scoring function used for \mathcal{D}_1 by an inner product, since it dramatically reduces the memory requirements and worked better in our case.

5 Experimental Methodology

5.1 Datasets

We evaluated the performance of GIC using seven commonly used benchmark datasets, whose statistics can be found in the Supplementary Material. Briefly, CORA [8], CiteSeer [31], and PubMed [32] are three citation networks, CoauthorCS and CoauthorPhysics [33] are co-authorship graphs, and AmazonComputer and AmazonPhoto [33] are segments of the Amazon co-purchase graph [34].

5.2 Node classification

The goal is to predict some (or all) of the nodes' labels based on a given (small) training set. In unsupervised methods, the learned node embeddings are passed to a downstream classifier, e.g., logistic regression. Following [33], we sample $20 \times \# \text{classes}$ nodes as the train set, $30 \times \# \text{classes}$ nodes as the validation set, and the remaining nodes are the test set. The sets are either uniformly drawn from each class (balanced sets) or randomly sampled (imbalanced sets). For the unsupervised methods, we use a logistic regression classifier, which is trained with a learning rate of 0.01 for 1k epochs with Adam SGD optimizer [35] and Glorot initialization [36]. The classification accuracy (Acc) is reported as a performance metric, which is the percentage of correctly classified instances $(\text{TP} + \text{TN}) / (\text{TP} + \text{TN} + \text{FP} + \text{FN})$ where TP, FN, FP, and TN represent the number of true positives, false negatives, false positives, and true negatives, respectively. The final results are averaged over 20 times. Following [33], we set the embedding dimensions $F' = 64$.

5.3 Link prediction

In link prediction, some edges are hidden in the input graph and the goal is to predict the existence of these edges based on the computed embeddings. The probability of an edge between nodes i and j is given by $\sigma(\mathbf{h}_i^T \mathbf{h}_j)$, where σ is the logistic sigmoid function. We follow the setup described in [3, 24]: 5% of edges and negative edges as validation set, 10% of edges and negative edges as test set, $F' = 16$, and the results are averaged over 10 runs. We report the area under the ROC curve (AUC) score [37], which is equal to the probability that a randomly chosen edge is ranked higher than a randomly chosen negative edge, and the average precision (AP) score [38], which is the area under the precision-recall curve; here, precision is given by $\text{TP}/(\text{TP}+\text{FP})$ and recall by $\text{TP}/(\text{TP}+\text{FN})$.

5.4 Clustering

In clustering, the goal is to cluster together related nodes (e.g., nodes that belong to the same class) without any label information. The computed embeddings are clustered into $K = \#\text{classes}$ clusters with K -means. The evaluation is provided by external labels, the same used for node classification. We report the classification accuracy (Acc), normalized mutual information (NMI), and average rand index (ARI) [39, 40]. NMI is an information-theoretic metric, while ARI can be viewed as an accuracy metric which additionally penalizes incorrect decisions. We set $F' = 32$, since most state-of-art competing approaches are invariant to the embedding size choice [41].

5.5 Hyper-parameter tuning and model selection

Encoder. As an encoder function f_{GNN} we utilize a graph convolution network (GCN) [20] with the following propagation rule at layer l

$$\mathbf{H}^{(l+1)} = \sigma(\hat{\mathbf{D}}^{-\frac{1}{2}} \hat{\mathbf{A}} \hat{\mathbf{D}}^{-\frac{1}{2}} \mathbf{H}^{(l)} \Theta), \quad (10)$$

where $\hat{\mathbf{A}} = \mathbf{A} + \mathbf{I}_N$ is the adjacency matrix with self-loops, $\hat{\mathbf{D}}$ is the degree matrix of $\hat{\mathbf{A}}$, i.e., $\hat{D}_{ii} = \sum_j \hat{A}_{ij}$, $\Theta \in \mathbb{R}^{F \times F'}$ is a learnable matrix, $\sigma(\cdot)$ denotes a nonlinear activation (here PReLU [42]), and $\mathbf{H}^{(0)} = \mathbf{X}$.

Parameter selection. We use one-layer GCN-encoder ($l = 1$), as suggested by [4], and as a similarity function in Eq. (7), we employ the cosine similarity as suggested by [5], and we iterate the cluster updates in Eq. (6), Eq. (7) for 10 times. Since GIC’s cluster updates are performed in the unit sphere (cosine similarity), we row-normalize the embeddings before the downstream task.

GIC’s learnable parameters are initialized with Glorot initialization [36] and the objective is optimized using the Adam SGD optimizer [35] with a learning rate of 0.001. We train for a maximum of $2k$ epochs, but the training is terminated with early stopping if the training loss does not improve in 50 consecutive epochs. The model state is reset to the one with the best (lowest) training loss.

To study the effect of the hyperparameters, which are α , the regularization parameter of the two objective terms, β , that controls the softness of the clusters, and K , the number of clusters, an ablation study is first provided. Then, for each dataset-task pair, we perform model selection based on the validation set: We set $\alpha \in \{0.25, 0.5, 0.75\}$, $\beta = \{10, 100\}$ and $K \in \{32, 128\}$ to train the model, and keep the parameters’ triplet that achieved the best result on the validation set (accuracy metric for node classification, AUC for link prediction, and accuracy for clustering). After that, we continue with the *same* triplet for the rest runs.

5.6 Competing approaches

We compare the performance of GIC against fifteen unsupervised and six semi-supervised methods and variants; details can be found in the Supplementary Material. The results for all the competing methods, except DGI, were obtained directly from [33, 41]. For DGI, we report results based on the DGI implementation of Deep Graph Library [43] for node classification, and the original DGI implementation for link prediction and clustering. Oftentimes, we refer to GIC with $\alpha = 1$ in Eq. (3) as DGI, since it coincides with the original DGI model.

Table 1: Node classification accuracy (in %) of various datasets and for two different train/val sets: balanced and imbalanced. The datasets are randomly split in each run.

Train/Val. Sets	Unsupervised				Semi-supervised	
	GIC		DGI		Best Method	Worst Method
	Imbalanced	Balanced	Imbalanced	Balanced		
CORA	81.7 ±1.5	80.7 ±1.1	80.2 ±1.8	80.0 ±1.3	81.8 ±1.3 (GAT)	76.6 ±1.9 (GS-maxpool)
CiteSeer	71.9 ±1.4	70.8 ±2.0	71.5 ±1.3	70.5 ±1.2	71.9 ±1.9 (GCN)	67.5 ±2.3 (GS-maxpool)
PubMed	77.3 ±1.9	77.4 ±1.9	76.2 ±2.0	76.8 ±2.3	78.7 ±2.3 (GAT)	76.1 ±2.3 (GS-maxpool)
CoauthorCS	89.4 ±0.4	89.3 ±0.7	89.0 ±0.4	88.7 ±0.8	91.3 ±2.3 (GS-mean)	85.0 ±1.1 (GS-maxpool)
CoauthorPhysics	93.1 ±0.7	92.4 ±0.9	92.7 ±0.8	91.8 ±1.0	93.0 ±0.8 (GS-mean)	90.3 ±1.2 (GS-maxpool)
AmazonComputers	81.5 ±1.0	79.5 ±1.4	79.0 ±1.7	77.9 ±1.8	83.5 ±2.2 (MoNet)	78.0 ±19.0 (GAT)
AmazonPhoto	90.4 ±1.0	89.0 ±1.6	88.2 ±1.7	86.8 ±1.7	91.4 ±1.3 (GS-mean)	85.7 ±20.3 (GAT)

Results are reported on the largest connected component (LCC) of the input graph.

Semi-supervised methods: GCN [20], GAT [21], GraphSAGE (GS) [2], and MoNet [44].

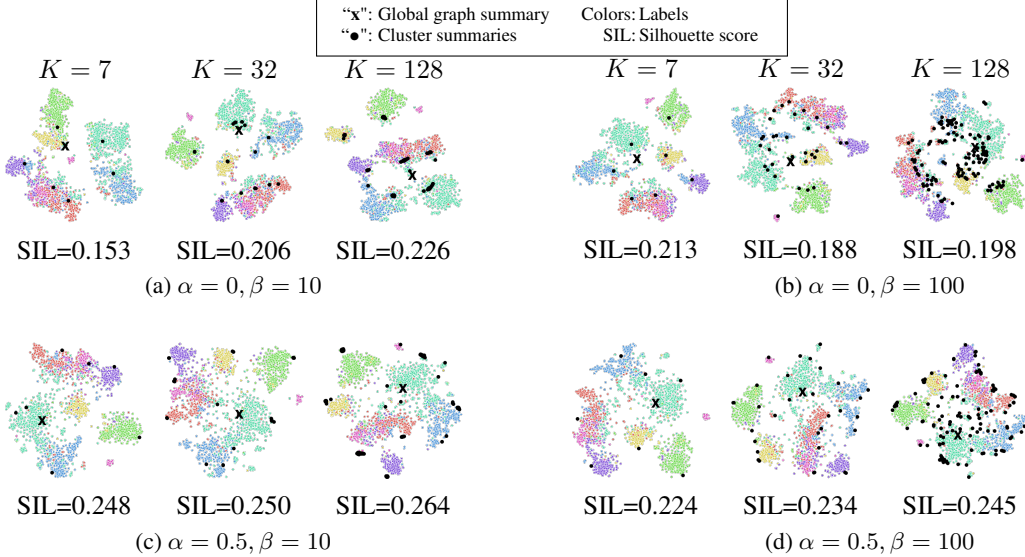


Figure 4: t-SNE plots for CORA dataset and the corresponding silhouette scores (SIL) with $\alpha \in \{0, 0.5\}$, $\beta \in \{10, 100\}$, $K \in \{\#\text{classes}, 32, 128\}$. The corresponding SIL score for DGI ($\alpha = 1$) is 0.212.

Table 2: Link prediction scores: Area Under Curve (AUC) score and Average Precision (AP) score (in %).

	CORA		Citeseer		PubMed	
	AUC	AP	AUC	AP	AUC	AP
Spectral Clustering [45]	84.6 ± 0.01	88.5 ± 0.00	80.5 ± 0.01	85.0 ± 0.01	84.2 ± 0.02	87.8 ± 0.01
DeepWalk [1]	83.1 ± 0.01	85.0 ± 0.00	80.5 ± 0.02	83.6 ± 0.01	84.4 ± 0.00	84.1 ± 0.00
VGAE [3]	91.4 ± 0.01	92.6 ± 0.01	90.8 ± 0.02	92.0 ± 0.02	96.4 ± 0.00	96.5 ± 0.00
ARGVA [41]	92.4 ± 0.004	93.2 ± 0.003	92.4 ± 0.003	93.0 ± 0.003	96.8 ± 0.001	97.1 ± 0.001
DGI [4]	89.8 ± 0.8	89.7 ± 1.0	95.5 ± 1.0	95.7 ± 1.0	91.2 ± 0.6	92.2 ± 0.5
GIC	93.5 ± 0.6	93.3 ± 0.7	97.0 ± 0.5	96.8 ± 0.5	93.7 ± 0.3	93.5 ± 0.3

For VGAE and ARGVA, we report their best performing variant for each dataset-metric pair: four and six total variants, respectively.

For DGI only, we set $F' = 32$ which greatly improves its results compared to $F' = 16$.

6 Experimental results

6.1 Ablation Study

In Figure 4, we plot the t-SNE 2D projection [7] of the learned node representations for the CORA dataset and $F' = 64$, and use silhouette scores (SIL) [6] to evaluate the results. SIL is the mean silhouette coefficient of all nodes, where the silhouette coefficient of each node n_i is a function of (i) the average distance between n_i and all other nodes with the same label and (ii) the lowest average distance of n_i to all nodes in any other label. Here, these distances are computed in the 2D projected space.

As illustrated in Figure 4, parameter α (which controls the relative importance of the two objective terms) tends to lead the optimized cluster summaries to show a certain behavior: A larger α pushes these summaries far from the center of the embedding space, while $\alpha = 0$ usually leads them to be near the center. For example, when comparing Figure 4c ($K = 128$) to Figure 4a ($K = 128$), most cluster summaries are spread to the borders of the embedding space (which also achieves a better SIL score).

With alternating parameter β , the distance between two cluster summaries is affected. A large β , e.g., $\beta = 100$, makes these distances larger than a smaller one, e.g., $\beta = 10$. For example, when comparing Figure 4d ($K = 128$) to Figure 4c ($K = 128$), for $\beta = 100$, the cluster summaries are more well-located in the embedding space, while for $\beta = 10$, we observe that most of them coincide.

Although increasing K generally helps, e.g., Figure 4a ($K = 128$) compared to Figure 4a ($K = 7$), the choice of K is not independent on the choice of α, β : Figure 4b is a counterexample that $K = 7$ achieved the best SIL score.

Table 3: Clustering results with respect to the true labels.

	CORA			CiteSeer			PubMed		
	Acc	NMI	ARI	Acc	NMI	ARI	Acc	NMI	ARI
<i>K</i> -means	49.2	31.1	23.0	54.0	30.5	27.9	39.8	0.1	0.2
DeepWalk [1]	48.4	32.7	24.3	33.7	8.8	9.2	68.4	27.9	29.9
DNGR [16]	41.9	31.8	14.2	32.6	18.0	4.4	45.8	15.5	5.4
TADW [46]	56.0	44.1	33.2	45.5	29.1	22.8	35.4	0.1	0.1
VGAE [3]	60.9	43.6	34.7	40.8	17.6	12.4	67.2	27.7	27.9
ARGVA [41]	71.1	52.6	49.5	58.1	33.8	30.1	69.0	30.5	30.6
DGI [4]	59.0 (71.3)	38.6 (56.4)	33.6 (51.1)	57.9 (68.8)	30.9 (44.4)	27.9 (45.0)	49.9 (53.3)	15.1 (18.1)	14.5 (16.6)
GIC	72.5	53.7	50.8	69.6	45.3	46.5	67.3	31.9	29.1

Acc: accuracy, NMI: normalized mutual information, ARI: average rand index in percents (%).

For VGAE and ARGVA, we report their best performing variant for each dataset-metric pair: four and six total variants, respectively.

For DGI, we also provide results in parentheses for $F' = 512$ (CORA and CiteSeer) and $F' = 128$ (PubMed), as reference.

Generally, we found that setting α close to values of 0.5 achieves better results $\alpha = 0$ or $\alpha = 1$ (see Supplementary Material). Finally, we observe the same behaviour based on β and K values in larger datasets, i.e., PubMed, as shown in the Supplementary Material.

6.2 Comparison against competing approaches

Node classification. GIC against DGI for the task of node classification and we present the results in Table 1. As we can see, GIC outperforms DGI in all datasets. In CORA and PubMed, GIC achieves a mean classification accuracy gain of more than 1%. In CiteSeer, CoauthorCS and CoauthorPhysics, the gain is slightly lower, but still more than 0.4%, on average. In AmazonComputers and AmazonPhoto, GIC performs significantly better than DGI with a gain of more than 2%, on average. Moreover, GIC’s performance lies always in between the best and worst performing semi-supervised method. In all cases, GIC performs better than the worst performing semi-supervised method with a gain of more than 1.5% and as high as 4.3%. Finally, as it is later demonstrated, GIC achieves even higher gains over DGI in cases like clustering, where the downstream model does not have access to the labels.

Link prediction. Table 2 illustrates the benefits of GIC over DGI for link prediction tasks. GIC outperforms DGI in all three datasets, by around 3.5% in CORA, 1.5% in CiteSeer, and 2.5% in PubMed, even though GIC’s embedding size is half of DGI’s. GIC also outperforms VGAE and ARGVA, in CORA and CiteSeer by 1%–2% and 4.5%–5.5%, respectively. In PubMed, the performance of GIC and DGI is worse than that of VGAE and ARGVA. We believe this is because reconstruction-based methods overestimate the existing node links (they reconstruct the adjacency matrix), which favors datasets like PubMed (this is not the case for CORA and CiteSeer which have significantly more attributes to exploit).

Clustering. Table 3 illustrates GIC’s performance for clustering. GIC performs better than other unsupervised methods in two out of three datasets, except for PubMed, where ARGVA works slightly better (however, we note that GIC outperforms five out of six ARGVA variants in this dataset). The gain over DGI is significantly large in all datasets, and can be as high as 15% to 18.5% for the NMI metric. GIC outperforms DGI in most metrics and datasets, even though DGI uses 16 times the embedding size of GIC ($F' = 512$).

7 Conclusion

We have presented Graph InfoClust (GIC), an unsupervised graph representation learning method which relies on leveraging cluster-level content. GIC identifies nodes with similar representations, clusters them together, and maximizes their mutual information. This enables us to improve the quality of node representations with richer content and obtain better results than existing approaches for tasks like node classification, link prediction, clustering, and data visualization.

References

- [1] Bryan Perozzi, Rami Al-Rfou, and Steven Skiena. Deepwalk: Online learning of social representations. In *Proceedings of the 20th ACM SIGKDD international conference on Knowledge discovery and data mining*, pages 701–710, 2014.
- [2] Will Hamilton, Zhitao Ying, and Jure Leskovec. Inductive representation learning on large graphs. In *Advances in neural information processing systems*, pages 1024–1034, 2017.
- [3] Thomas N Kipf and Max Welling. Variational graph auto-encoders. *NIPS Workshop on Bayesian Deep Learning*, 2016.
- [4] Petar Veličković, William Fedus, William L. Hamilton, Pietro Liò, Yoshua Bengio, and R Devon Hjelm. Deep Graph Infomax. In *International Conference on Learning Representations*, 2019.
- [5] Bryan Wilder, Eric Ewing, Bistra Dilkina, and Milind Tambe. End to end learning and optimization on graphs. In *Advances in Neural and Information Processing Systems*, 2019.
- [6] Peter J Rousseeuw. Silhouettes: a graphical aid to the interpretation and validation of cluster analysis. *Journal of computational and applied mathematics*, 20:53–65, 1987.
- [7] Laurens van der Maaten and Geoffrey Hinton. Visualizing data using t-sne. *Journal of machine learning research*, 9(Nov):2579–2605, 2008.
- [8] Andrew Kachites Mccallum, Kamal Nigam, Jason Rennie, and Kristie Seymore. Automating the construction of internet portals with machine learning. *Information Retrieval*, 3:127–163, 2000.
- [9] Mikhail Belkin and Partha Niyogi. Laplacian eigenmaps for dimensionality reduction and data representation. *Neural computation*, 15(6):1373–1396, 2003.
- [10] Amr Ahmed, Nino Shervashidze, Shravan Narayananurthy, Vanja Josifovski, and Alexander J Smola. Distributed large-scale natural graph factorization. In *Proceedings of the 22nd international conference on World Wide Web*, pages 37–48, 2013.
- [11] Shaosheng Cao, Wei Lu, and Qiongkai Xu. Grarep: Learning graph representations with global structural information. In *Proceedings of the 24th ACM international conference on information and knowledge management*, pages 891–900, 2015.
- [12] Mingdong Ou, Peng Cui, Jian Pei, Ziwei Zhang, and Wenwu Zhu. Asymmetric transitivity preserving graph embedding. In *Proceedings of the 22nd ACM SIGKDD international conference on Knowledge discovery and data mining*, pages 1105–1114, 2016.
- [13] Aditya Grover and Jure Leskovec. node2vec: Scalable feature learning for networks. In *Proceedings of the 22nd ACM SIGKDD international conference on Knowledge discovery and data mining*, pages 855–864, 2016.
- [14] Jian Tang, Meng Qu, Mingzhe Wang, Ming Zhang, Jun Yan, and Qiaozhu Mei. Line: Large-scale information network embedding. In *Proceedings of the 24th international conference on world wide web*, pages 1067–1077, 2015.
- [15] Haochen Chen, Bryan Perozzi, Yifan Hu, and Steven Skiena. Harp: Hierarchical representation learning for networks. In *Thirty-Second AAAI Conference on Artificial Intelligence*, 2018.
- [16] Shaosheng Cao, Wei Lu, and Qiongkai Xu. Deep neural networks for learning graph representations. In *Thirtieth AAAI conference on artificial intelligence*, 2016.
- [17] Daixin Wang, Peng Cui, and Wenwu Zhu. Structural deep network embedding. In *Proceedings of the 22nd ACM SIGKDD international conference on Knowledge discovery and data mining*, pages 1225–1234, 2016.
- [18] James Atwood and Don Towsley. Diffusion-convolutional neural networks. In *Advances in neural information processing systems*, pages 1993–2001, 2016.
- [19] Mathias Niepert, Mohamed Ahmed, and Konstantin Kutzkov. Learning convolutional neural networks for graphs. In *International conference on machine learning*, pages 2014–2023, 2016.
- [20] Thomas N Kipf and Max Welling. Semi-supervised classification with graph convolutional networks. *arXiv preprint arXiv:1609.02907*, 2016.
- [21] Petar Veličković, Guillem Cucurull, Arantxa Casanova, Adriana Romero, Pietro Liò, and Yoshua Bengio. Graph Attention Networks. *International Conference on Learning Representations*, 2018.
- [22] Ziqi Liu, Chaochao Chen, Longfei Li, Jun Zhou, Xiaolong Li, Le Song, and Yuan Qi. Geniepath: Graph neural networks with adaptive receptive paths. In *Proceedings of the AAAI Conference on Artificial Intelligence*, volume 33, pages 4424–4431, 2019.

- [23] Zonghan Wu, Shirui Pan, Fengwen Chen, Guodong Long, Chengqi Zhang, and S Yu Philip. A comprehensive survey on graph neural networks. *IEEE Transactions on Neural Networks and Learning Systems*, 2020.
- [24] Shirui Pan, Ruiqi Hu, Guodong Long, Jing Jiang, Lina Yao, and Chengqi Zhang. Adversarially regularized graph autoencoder for graph embedding. In *Proceedings of the Twenty-Seventh International Joint Conference on Artificial Intelligence, IJCAI-18*, pages 2609–2615. International Joint Conferences on Artificial Intelligence Organization, 7 2018.
- [25] Ian Goodfellow, Jean Pouget-Abadie, Mehdi Mirza, Bing Xu, David Warde-Farley, Sherjil Ozair, Aaron Courville, and Yoshua Bengio. Generative adversarial nets. In *Advances in neural information processing systems*, pages 2672–2680, 2014.
- [26] William L Hamilton, Rex Ying, and Jure Leskovec. Representation learning on graphs: Methods and applications. *arXiv preprint arXiv:1709.05584*, 2017.
- [27] Claude E Shannon. A mathematical theory of communication. *Bell system technical journal*, 27(3):379–423, 1948.
- [28] Thomas M Cover and Joy A Thomas. *Elements of information theory*. John Wiley & Sons, 1991.
- [29] R Devon Hjelm, Alex Fedorov, Samuel Lavoie-Marchildon, Karan Grewal, Phil Bachman, Adam Trischler, and Yoshua Bengio. Learning deep representations by mutual information estimation and maximization. In *International Conference on Learning Representations*, 2019.
- [30] Aaron van den Oord, Yazhe Li, and Oriol Vinyals. Representation learning with contrastive predictive coding. *arXiv preprint arXiv:1807.03748*, 2018.
- [31] C. Lee Giles, Kurt D. Bollacker, and Steve Lawrence. Citeseer: an automatic citation indexing system. In *INTERNATIONAL CONFERENCE ON DIGITAL LIBRARIES*, pages 89–98. ACM Press, 1998.
- [32] Galileo Namata, Ben London, Lise Getoor, Bert Huang, and UMD EDU. Query-driven active surveying for collective classification. In *10th International Workshop on Mining and Learning with Graphs*, volume 8, 2012.
- [33] Oleksandr Shchur, Maximilian Mumme, Aleksandar Bojchevski, and Stephan Günnemann. Pitfalls of graph neural network evaluation. *arXiv preprint arXiv:1811.05868*, 2018.
- [34] Julian McAuley, Christopher Targett, Qinfeng Shi, and Anton van den Hengel. Image-based recommendations on styles and substitutes. In *Proceedings of the 38th International ACM SIGIR Conference on Research and Development in Information Retrieval, SIGIR ’15*, page 43–52, New York, NY, USA, 2015. Association for Computing Machinery.
- [35] Diederik P. Kingma and Jimmy Ba. Adam: A method for stochastic optimization, 2014.
- [36] Xavier Glorot and Yoshua Bengio. Understanding the difficulty of training deep feedforward neural networks. In Yee Whye Teh and Mike Titterington, editors, *Proceedings of the Thirteenth International Conference on Artificial Intelligence and Statistics*, volume 9 of *Proceedings of Machine Learning Research*, pages 249–256, Chia Laguna Resort, Sardinia, Italy, 13–15 May 2010. PMLR.
- [37] Andrew P. Bradley. The use of the area under the roc curve in the evaluation of machine learning algorithms. *Pattern Recogn.*, 30(7):1145–1159, July 1997.
- [38] Wanhua Su, Yan Yuan, and Mu Zhu. A relationship between the average precision and the area under the roc curve. In *Proceedings of the 2015 International Conference on The Theory of Information Retrieval, ICTIR ’15*, page 349–352, New York, NY, USA, 2015. Association for Computing Machinery.
- [39] Lawrence Hubert and Phipps Arabie. Comparing partitions. *Journal of classification*, 2(1):193–218, 1985.
- [40] Christopher D. Manning, Prabhakar Raghavan, and Hinrich Schütze. *Introduction to Information Retrieval*. Cambridge University Press, USA, 2008.
- [41] Shirui Pan, Ruiqi Hu, Sai-fu Fung, Guodong Long, Jing Jiang, and Chengqi Zhang. Learning graph embedding with adversarial training methods. *IEEE transactions on cybernetics*, 2019.
- [42] Kaiming He, Xiangyu Zhang, Shaoqing Ren, and Jian Sun. Delving deep into rectifiers: Surpassing human-level performance on imagenet classification. In *Proceedings of the IEEE international conference on computer vision*, pages 1026–1034, 2015.
- [43] Minjie Wang, Lingfan Yu, Da Zheng, Quan Gan, Yu Gai, Zihao Ye, Mufei Li, Jinjing Zhou, Qi Huang, Chao Ma, Ziyue Huang, Qipeng Guo, Hao Zhang, Haibin Lin, Junbo Zhao, Jinyang Li, Alexander J Smola, and Zheng Zhang. Deep graph library: Towards efficient and scalable deep learning on graphs. *ICLR Workshop on Representation Learning on Graphs and Manifolds*, 2019.

- [44] Federico Monti, Davide Boscaini, Jonathan Masci, Emanuele Rodola, Jan Svoboda, and Michael M Bronstein. Geometric deep learning on graphs and manifolds using mixture model cnns. In *Proceedings of the IEEE Conference on Computer Vision and Pattern Recognition*, pages 5115–5124, 2017.
- [45] Lei Tang and Huan Liu. Leveraging social media networks for classification. *Data Mining and Knowledge Discovery*, 23(3):447–478, 2011.
- [46] Cheng Yang, Zhiyuan Liu, Deli Zhao, Maosong Sun, and Edward Chang. Network representation learning with rich text information. In *Twenty-Fourth International Joint Conference on Artificial Intelligence*, 2015.
- [47] Prithviraj Sen, Galileo Namata, Mustafa Bilgic, Lise Getoor, Brian Galligher, and Tina Eliassi-Rad. Collective classification in network data. *AI magazine*, 29(3):93–93, 2008.
- [48] Zhilin Yang, William W. Cohen, and Ruslan Salakhutdinov. Revisiting semi-supervised learning with graph embeddings. In *Proceedings of the 33rd International Conference on International Conference on Machine Learning - Volume 48*, ICML’16, page 40–48. JMLR.org, 2016.
- [49] Adam Paszke, Sam Gross, Soumith Chintala, Gregory Chanan, Edward Yang, Zachary DeVito, Zeming Lin, Alban Desmaison, Luca Antiga, and Adam Lerer. Automatic differentiation in pytorch. 2017.

Table 4: Datasets statistics; whole graph and largest connected component (LCC) of the graph as reported in [33].

	Classes	Features	Nodes	Edges	Label rate	Nodes LCC	Edges LCC	Label rate LCC
CORA	7	1,433	2,708	6,632	0.0517	2,485	5,069	0.0563
CiteSeer	6	3,703	3,327	4,614	0.0324	2,110	3,668	0.0569
PubMed	3	500	19,717	44,324	0.0030	19,717	44,324	0.0030
CoauthorCS	15	6,805	18,333	81,894	0.0164	18,333	81,894	0.0164
CoauthorPhysics	5	8,415	34,493	247,962	0.0029	34,493	247,962	0.0029
AmazonComputer	10	767	13,752	287,209	0.0145	13,381	245,778	0.0149
AmazonPhoto	8	745	7,650	143,663	0.0209	7,487	119,043	0.0214

Label rate is the fraction of nodes in the training set (train size equals to $20 \times \# \text{classes}$) for node classification tasks.

8 Supplementary Material

8.1 Datasets

We evaluated the performance of GIC using seven commonly used benchmark datasets (Table 4).

CORA, CiteSeer, and PubMed [47, 48] are three text classification datasets. Each dataset contains bag-of-words representation of documents as features and citation links between the documents as edges. The CORA dataset [8] contains a number of machine-learning papers divided into one of seven classes while the CiteSeer dataset [31] has six class labels. The PubMed dataset [32] consists of scientific publications from the PubMed database pertaining to diabetes classified into three classes.

CoauthorCS and CoauthorPhysics [33] are co-authorship graphs based on the Microsoft Academic Graph. Nodes are authors and edges represent co-authorship relations. Classes represent the most active fields of studies, and node features are the bag-of-words encoded paper keywords for each author’s papers.

AmazonComputer and AmazonPhoto [33] are segments of the Amazon co-purchase graph [34]. Nodes represent items and are classified into product categories, with their features to be bag-of-words encoded product reviews. Edges indicate that two items are frequently bought together.

8.2 Competing Approaches

We compare the performance of GIC against the following unsupervised methods and baselines.

- Deep Graph Infomax (DGI) [4]
- Variational Graph Auto-Encoders (GAE*/VGAE* and GAE/VGAE) [3]
- Adversarially Regularized Graph Autoencoder (ARGVA) [41], and its variants ARGA, ARGA-DG, ARGVA-DG, ARGA-AX, and ARGVA-AX
- DeepWalk [1], Text-Associated DeepWalk (TADW) [46]
- Deep Neural Network for Graph Representation (DNGR) [16]
- Spectral Clustering [45]

Representative GNN unsupervised methods that rely on both structure and features include GAE/VGAE, which are well-known reconstruction-based methods, and ARGVA and its variants, which additionally learn the data distribution in an adversarial fashion. GAE*/VGAE*, Spectral Clustering, DeepWalk, and DNGR rely only on graph structure. TADW is a version of DeepWalk that additionally accounts for features.

To evaluate how GIC’s unsupervised representations compared to semi-supervised approaches that use the labels during representation learning, we used the following semi-supervised approaches.

- Graph Convolutional Network (GCN) [20]
- Graph Attention Network (GAT) [21]
- Mixture Model Network (MoNet) [44]
- GraphSAGE (GS) [2], and its aggregator types GS-mean, GS-meanpool, GS-maxpool

which are well-known GNN-based methods.

α	β	K	CORA	CiteSeer	PubMed	α	β	K	CORA	CiteSeer	PubMed
0	10	#classes	0.153	0.144	0.091	0.5	10	32	0.248	0.170	0.110
0	10	32	0.206	0.140	0.094	0.5	10	128	0.250	0.176	0.111
0	10	128	0.226	0.165	0.081	0.5	10	#classes	0.264	0.158	0.113
0	100	#classes	0.213	0.144	0.086	0.5	100	32	0.224	0.148	0.115
0	100	32	0.188	0.173	0.092	0.5	100	128	0.234	0.153	0.107
0	100	128	0.198	0.172	0.091	0.5	100	#classes	0.245	0.170	0.105
0.25	10	#classes	0.216	0.146	0.099	0.75	10	32	0.243	0.160	0.125
0.25	10	32	0.253	0.157	0.102	0.75	10	128	0.243	0.125	0.119
0.25	10	128	0.223	0.173	0.099	0.75	100	#classes	0.250	0.166	0.114
0.25	100	#classes	0.236	0.172	0.066	0.75	100	32	0.236	0.161	0.115
0.25	100	32	0.239	0.177	0.101	0.75	100	128	0.244	0.165	0.105
0.25	100	128	0.232	0.165	0.102	0.75	100	#classes	0.225	0.159	0.102
						1	-	-	0.191	0.145	0.077

Table 5: Silhouette scores of the t-SNE 2D projections of the learned node representations, based on different hyperparameter α, β, K values. Bold font indicates the two best scores for each dataset.

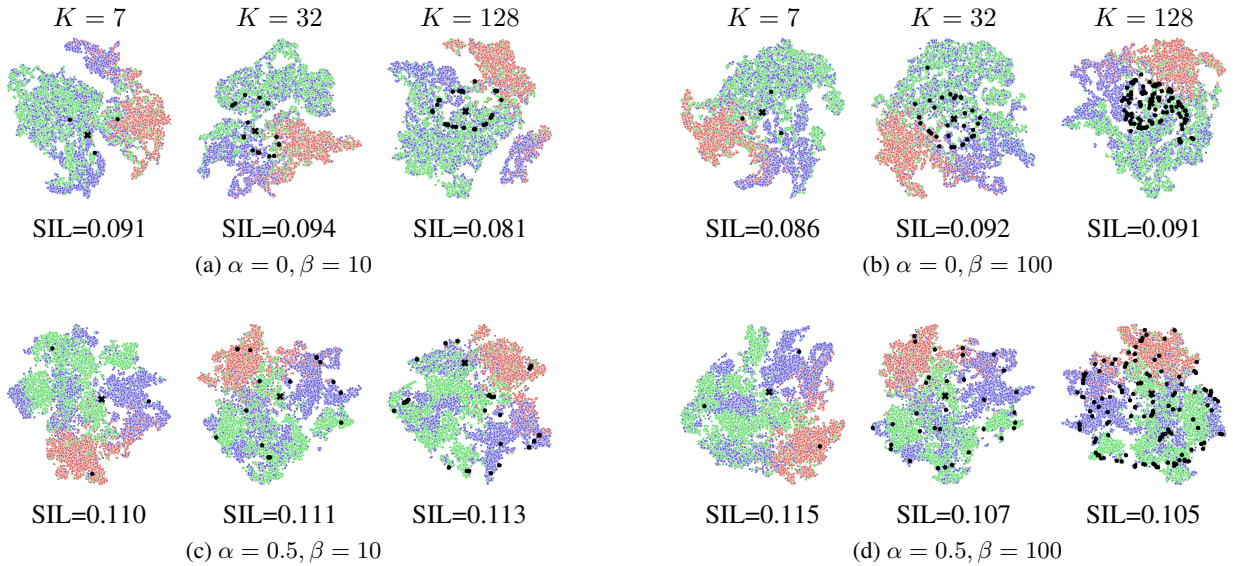


Figure 5: t-SNE plots for PubMed dataset and the corresponding silhouette scores (SIL) with $\alpha \in \{0, 0.5\}$, $\beta \in \{10, 100\}$, $K \in \{\#\text{classes}, 32, 128\}$. The corresponding SIL score for DGI ($\alpha = 1$) is 0.077.

8.3 Hardware and software

We implemented GIC using the Deep Graph Library [43] and PyTorch [49] (the code will be made publicly available after the paper is accepted). We also implemented GIC by modifying DGI’s original implementation¹, which we use in some experiments, e.g., link prediction and clustering. All experiments were performed on a Nvidia Geforce RTX-2070 GPU on a i5-8400 CPU and 32GB RAM machine.

8.4 Additional experiments

The additional experiments are part of the Ablation Study section. In Table 5, we present silhouette scores (SIL) for different datasets, based on different hyperparameter α, β, K values. In Figure 5, we also plot the learned node representations for PubMed dataset, after t-SNE 2D projection is applied.

¹DGI implementations are found in <https://github.com/dmlc/dgl/tree/master/examples/pytorch/dgi> and <https://github.com/PetarV-/DGI>.